

Conductive-AFM topography and current maps simulator for the study of polycrystalline high-k dielectrics

Carlos Couso^{a)}, M. Porti, J. Martin-Martinez, V. Iglesias, M. Nafria and X. Aymerich.

Dept. Enginyeria Electronica, Universitat Autònoma de Barcelona (UAB), 08193 Bellaterra, Spain.

^{a)} Electronic mail: carlos.couso@uab.cat

In this work, a simulator of Conductive Atomic Force Microscopy (C-AFM) was developed to reproduce topography and current maps. In order to test the results, we used the simulator to investigate the influence of the C-AFM tip on topography measurements of polycrystalline high-k dielectrics, and compared the results with experimental data. The results show that this tool can produce topography images with the same morphological characteristics as the experimental samples under study. Additionally, the current at each location of the dielectric stack was calculated. The Quantum Mechanical Transmission Coefficient (QMTC) and tunneling current were obtained from the band diagram by applying the Airy wavefunction approach. Good agreement between experimental and simulation results indicates that the tool can be very useful for evaluating how the experimental parameters influence C-AFM measurements.

I. INTRODUCTION

High-k materials are applied as gate dielectrics for current and emerging technologies. However, several issues impede the complete optimization of these materials. One of the most relevant concerns is polycrystallization of the high-k material after thermal annealing, which increases the leakage current and its variability in ultrascaled devices.¹⁻³

High-k polycrystallization takes place at the nanometer scale, and therefore, a complete characterization of this phenomenon is required. In this context, C-AFM has been demonstrated to be a very powerful technique to evaluate the topographic and electrical properties of high-k dielectrics at the nanoscale.^{4,5} In particular, this technique was successfully used in several studies to evaluate the impact of polycrystallization.⁵⁻⁷ One of the most relevant conclusions of these works was that, in polycrystalline HfO₂ layers, the gate leakage current mainly flows through grain boundaries (GBs). This is because of the reduced oxide thickness at these sites and the variation in electrical properties at the GBs, which are related to an excess of oxygen vacancies.⁵ However, several intrinsic factors of the C-AFM technique, such as the tip conductivity and shape, and its progressive wear unavoidably affect the measurements, leading in some cases to erroneous results. Evaluating how these factors influence measurements can be complicated or nearly impossible in many cases if only C-AFM is used. To deal with this problem, a C-AFM simulator has been developed. Our simulation tool takes into account the morphology and electrical properties of a high-k dielectric in contact with a sharp conductive tip, reproducing the conditions of a C-AFM characterization. Using this approach, problematic factors, such as the tip geometry or others can be analyzed and their impact on the C-AFM measurements studied in detail.

In order to test the simulator, its output was compared to C-AFM experimental data obtained for a polycrystalline high-k dielectric.⁵ Particularly, topographical maps were measured with a C-AFM working in contact mode. Metallic-coated silicon tips were used for these measurements. The stack under analysis has the following structure: HfO₂ film

with a nominal thickness of 5 nm, deposited by atomic layer deposition on a native 1-nm thick SiO₂ layer. The dielectric stack was grown on a p-type Si epitaxial substrate.

II. MODELLING

To develop the simulator, two different modules have been considered. The topography module, which reproduces the high-k morphology when measured with C-AFM, and the current module, which calculates the tunneling current through the high-k stack at each point from the map obtained with the topography module.

A. Topography module

To perform a topography simulation, some input parameters related to the sample morphological properties must be provided. In our case, these parameters were extracted from C-AFM morphology measurements. In particular, for a polycrystalline structure, statistical geometrical parameters related to the grain size and the grain boundary (GB) width and depth (with respect to grains) are necessary. These parameters can be easily estimated from the statistical analysis of an experimental map (such as that in Fig. 3a) by means of the open processing software.⁸ Table 1 shows, as an example, some parameters related to the sample morphology that can be obtained and that are of interest for our simulations. In the “experimental” column in Table 1, the mean and standard deviation (SD) are shown for different geometrical and topographical parameters obtained from the experimental image.

Parameter	Experimental		Simulated	
	Mean	SD	Mean	SD
Radius grains (nm)	33.2	8.2	38.5	11.3
Height grains (nm)	2.46	0.19	2.18	0.23
Width GB (nm)	3.3	1.4	2.1	1.2
Height GB (nm)	1.13	0.26	0.98	0.31

Table 1. Statistical parameters obtained from a polycrystalline HfO₂ layer (experimental columns) and the same parameters obtained from the simulated topographic maps (simulated columns).

These experimental parameters were used as input parameters for the simulator. The polycrystalline topography surface was generated by using Monte Carlo simulation through the acceptance-rejection method.⁹ Each grain was approximated to one polygon with n sides, randomly obtained between a minimum and a maximum (in this work, 8 and 15 were used, respectively), whose center also was randomly selected at a given position on the surface (P in Fig. 1). The distance of each side to the center P (R1 and R2 in Fig. 1a) and the angle between R1 and R2 were statistically estimated based on the experimental data obtained from topographical images (Fig. 1a). Then, the morphology of the GB surrounding the grain (Fig. 1b) also was estimated, using the experimental data shown in Table 1. This process was repeated until the surface simulation was full (Fig. 1c). Finally, the height of each grain and GB was calculated from the height probability inputs obtained from C-AFM experimental images.

As previously was explained, when surfaces are measured with C-AFM, the resulting topography is affected by the tip geometry. To investigate this point, a convolution algorithm¹⁰ was applied to the simulated surfaces, with the assumption that the tip has a semispherical shape. To validate this simulation technique, the resulting topography maps

were compared with experimental C-AFM images. Detailed results are provided in Section III. Next section is focused in the current module.

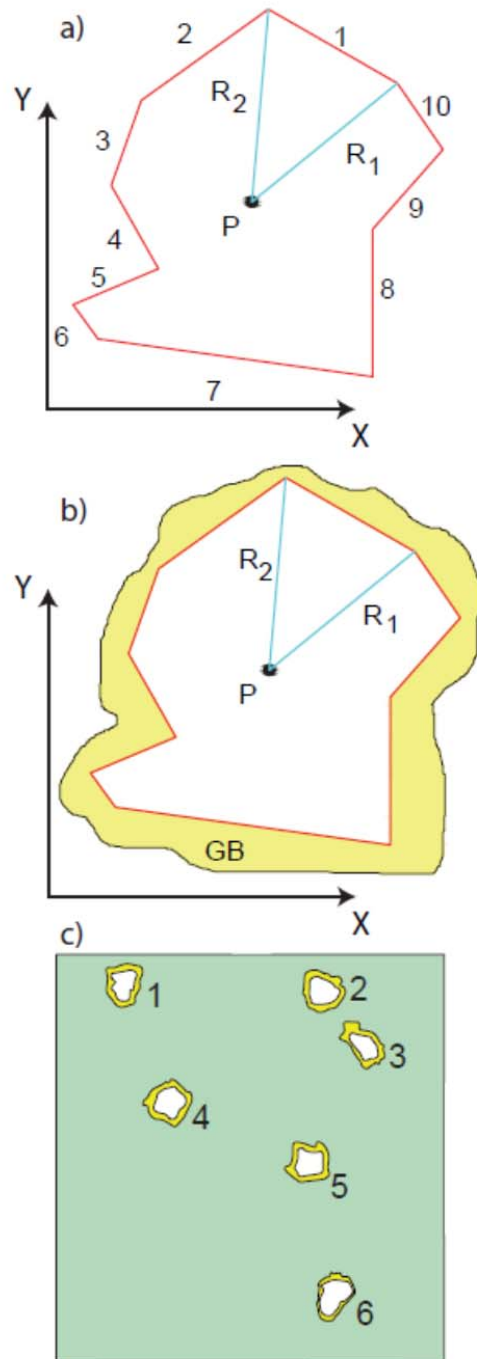


Figure 1. (a) Sketch of the process for creating one grain. (b) The surrounding GB. (c) Several grains and GBs were created on the simulation surface.

B. Current module

Once the simulated topographic map was obtained, a model was developed to simulate the current through the C-AFM tip. The following parameters were used as inputs: the oxide thickness at each point on the map, dielectric constant, barrier height, effective mass, the work function of the tip and the applied voltage. With these inputs, the structure band diagram can be calculated using open-source software.^{11,12} To determine the oxide thickness at each point, the simulator accounted for the statistical surface parameters of the top and bottom interfaces of the different layers of the stack. However, in this work, the SiO₂-HfO₂ interface was not experimentally measured because the SiO₂-HfO₂ interface roughness tends to be much lower than the HfO₂ superficial roughness. The native SiO₂ roughness also was neglected. Thus, only the roughness of the top HfO₂ surface is considered for our purposes.

To calculate the current, the size and shape of the tip also were considered, because not all the points of the tip apex are in contact with the sample (Fig. 2a). Consequently, for each point of the surface, the current were evaluated by considering the current through that site and also through the surrounding region. Fig. 2 shows an example of this approach. When the current is evaluated for a particular site of a surface (evaluated point in Fig. 2a), depending on the local topography, it is possible that the tip was not in contact with the “evaluated point.” This is because the tip could contact to a higher site: “contact point.” At the “contact points,” the band diagram in Fig. 2b was considered. In the sites without contact (non-contact points), the band diagram was added to a gap with a barrier height that depended on the considered environment (vacuum, N₂, atmosphere, etc.) and a thickness (H) equal to the distance between the tip and that site (Fig. 2c).

Thus, all the sites below the C-AFM tip were considered when calculating the total current. Therefore, the tip geometry, sample topography and environment were taken into account for the current calculation.

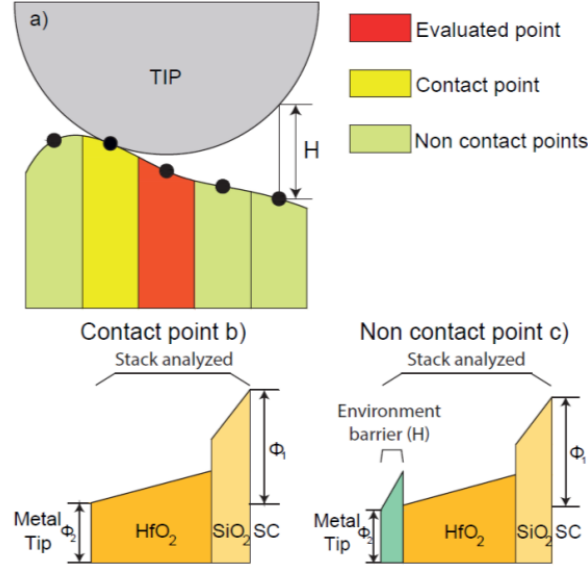


Figure 2. a) 2D Sketch of a tip on a surface. Several contact conditions between tip and sample can result. b) Band diagram for a contact point. c) Band diagram with extra barrier due to the environment effect at the “non-contact points.”

From the band diagram at each site, the Quantum Mechanical Transmission Coefficient (QMTC) can be calculated by applying the Airy wavefunction approach.¹³ In order to solve any barrier shape, the algorithm has been implemented by means of a transfer-matrix procedure.^{14,15} Finally, the current density at each point was calculated using the following expression:¹⁶

$$J_z = \frac{e \sum_l n_v m_{dl}}{2\pi^2 \hbar^3} \int_0^\infty T(E_z) kT \ln \left\{ \frac{(1 + \exp[(E_F - E_z)/kT])^\lambda}{1 + \exp[(E_F - E_z - (eV_{ox} - \Delta))/kT]} \right\} dE_z, \quad (1)$$

where e is the electron charge, l is the valley number, n_v is the valley degeneracy, m_d is the density-of-states mass per valley, \hbar is the reduced Planck constant, $T_e(E_z)$ is the

electron transmittance, E_z is the electron energy perpendicular to the sample surface, k is the Boltzmann constant, T is the temperature, E_F is the Fermi level and V_{ox} is the oxide voltage. The term λ is expressed as $\lambda = m_{ta,e}/m_{tb,e}$, which is the ratio between the transverse effective mass in the tip, $m_{ta,e}$, and that in the conduction band edge of the silicon substrate, $m_{tb,e}$, where $m_{ta,e} = \sum |n_v| m_{dl}$.

III. RESULTS AND DISCUSSION

A. Topography results

Fig. 3a shows an experimental topography map of a HfO₂ polycrystalline layer with a nominal thickness of 5 nm measured using the C-AFM technique. From this experimental map, the necessary parameters were calculated and introduced as inputs in the simulator (Table 1 experimental columns). Fig. 3b shows a simulated topographic map obtained from the extracted parameters of the experimental image (Fig. 3a). Note that both images show grains with similar sizes and random shapes, (see highlighted grains in both maps). However, it is important to emphasize that the algorithms used to generate the polygons (i. e., the grains in the simulated image) and to take into account the convolution with the CAFM tip are not directly related to any experimental parameter. Therefore, they should be quantitatively validated. To do so, the experimental statistical parameters shown in Table 1 have been compared to those obtained from the simulated map (Table 1 simulated columns). Note that, when the standard deviations are considered, fairly good agreement was observed. Moreover, the thickness cumulative distributions of the experimental maps (Fig. 3a) and several of the simulated maps are plotted in Fig. 3c. The black line represents the data corresponding to the experimental map and the color lines

correspond to the simulated maps. The different simulated maps were obtained by inputting the same statistical parameters (obtained from Fig. 3a) but changing the simulation random seed. Note that all the simulated thickness cumulative distributions are very similar to the experimental one. The small differences can be related to the fact that different seeds and, therefore, different random areas are simulated which, although being similar from a statistical point of view, are not identical (as expected). The good match between the experimental and simulated statistical parameters (shown in Table 1) and the distributions obtained from experimental and simulated maps indicates that the proposed simulation methodology accurately reproduces the topography of polycrystalline structures.

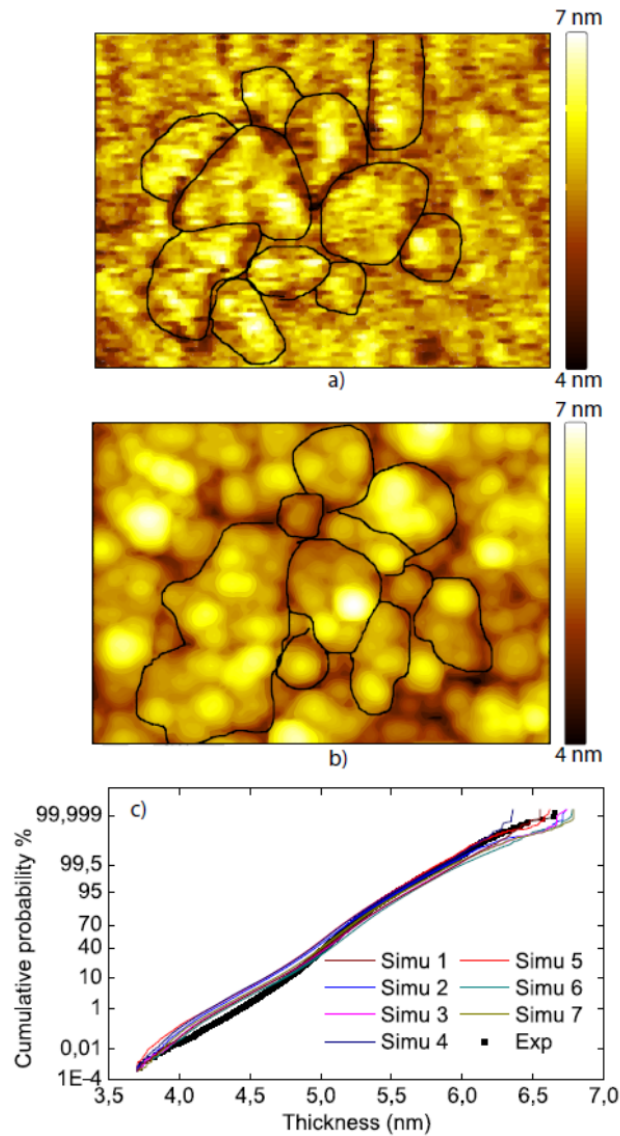


Figure 3. Experimental (a) and simulated (b) topography images of $\text{HfO}_2/\text{SiO}_2/\text{Si}$ structure (area of $400 \times 300 \text{ nm}^2$). (c) Thickness cumulative probability obtained from the experimental (black) and several simulated (colors) topography maps. Various simulation random seeds are used for the simulations.

Once the simulator has been checked, the influence of experimental factors such as the tip radius, environment or tip shape can be evaluated separately. As an example, in this manuscript, the impact of the AFM tip radius on the topography measurements was investigated. Fig. 4 shows the roughness (RMS) obtained from experimental (black triangles) and simulated (empty color squares) topographical maps. To obtain the

experimental data, several topography maps of the same sample were measured using tips with different radii. The simulated data were obtained by inputting the parameters extracted from the experimental image shown in Fig. 3a and varying the radius parameter. Both the experimental and simulated images show that the tip radius affects the observed roughness. Specifically, when the tip radius is increased, the roughness of the surface decreases, as expected. However, the roughness is a parameter strongly dependent on the mean depth of the GB. Therefore, simulations were performed with varying mean depths (μ_{GBdepth}), as shown in the plot. The best match between the simulations and experimental data was obtained at a mean GB depth of 1.3 nm. This example shows that this type of simulations can be used to evaluate how the C-AFM tip affects topography measurements and get a more accurate picture of the surface under study.

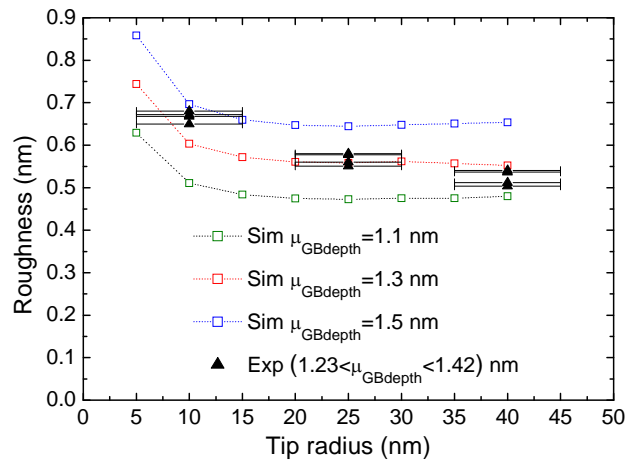


Figure 4. Roughness as a function of tip radius. Simulations were performed for various GB depths.

B. Current results

After the topography of the polycrystalline HfO₂ layer was simulated, the current through the stack under study was determined following the procedure described in section II.B. A 5-nm HfO₂/1 nm SiO₂/Si p-type stack was simulated, i.e., the same structure that was experimentally measured. Fig. 5a shows the QMTC as a function of the electron energy at a contact point (black) and a non-contact point (red) with an extra barrier of 0.5 nm associated with an air environment. The QMTC decreases quickly if there is a gap related to the environment, as expected. Therefore, from Fig. 5a it is evident that tunneling transport occurs preferentially through the contact point. These results emphasize that a good contact between the sample and tip must be ensured to avoid appearance of an extra barrier that could modify the current obtained through the stack. Fig. 5b represents the QMTC at two sites of differing physical natures (a 6.2-nm thick grain and a 4.5-nm thick GB). Note that the transmittance is higher for a GB and, consequently, larger current should be expected there. These results are confirmed in the simulated and experimental current maps in Figs. 6a and 6b.

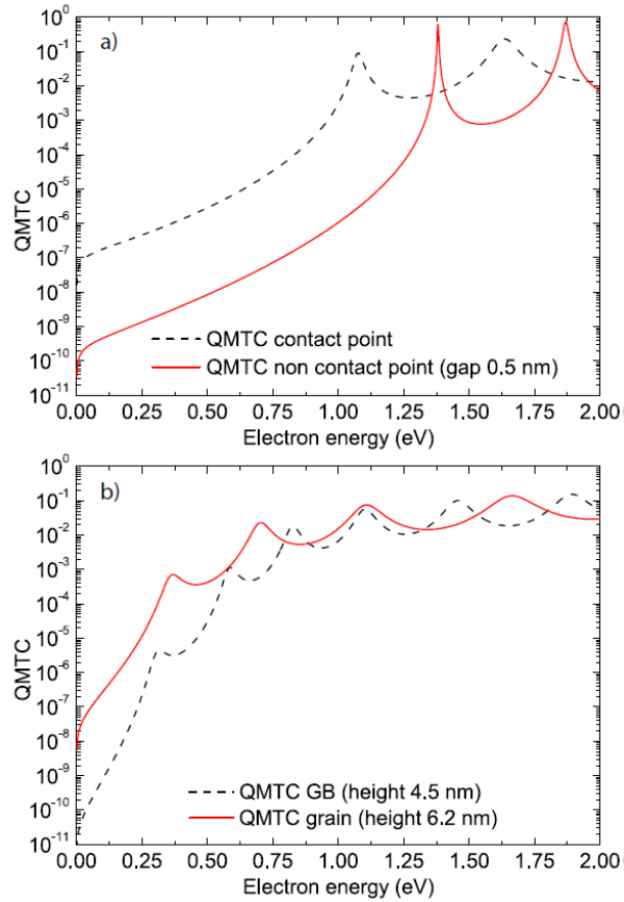


Figure 5. The QMTC as function of electron energy with bias equal to 1 V. a) Difference between a contact point and a non-contact point (environment gap of 0.5 nm). b) Difference between a grain (6.2-nm height) and at a grain boundary (4.5-nm height).

Figures 6a and 6b show an experimental (a) and simulated (b) current map, which correspond to the structures whose topography maps are shown in Fig. 3a and 3b, respectively. Note that, in both cases, the current flows preferentially through the GBs and higher currents are obtained at the GBs (thinner regions). To analyze the relation between the current level and the depth of the GBs, the current as a function of HfO₂ thickness, obtained from different experimental maps and simulated surfaces, is plotted in Fig. 6c and d, respectively. Areas larger than those shown in Figs. 3 and 6 have been considered, so that the analysis is statistically meaningful. Note that in Fig. 6d

(corresponding to simulated data) a clear relation between current and gate stack thickness is observed, as expected. However, there is not a univocal correspondence between current and thickness. This is because the current does not depend on the layer thickness at a given site, but also on the contact characteristics. Therefore, other surrounding points could also contribute to the global current measured by the CAFM tip at a given site.

In Fig. 6c, corresponding to the experimental data, two clear regions can be distinguished. Above a thickness of approx. 6 nm, a constant current around 1 pA is registered, which corresponds basically to the noise level of the CAFM. Below 6 nm, the relation between the current and the oxide thickness is not as clear as in the simulated image⁵. Moreover, Fig. 6c also shows that experimental currents can be higher than the simulated currents. These differences could be explained because up to now, only differences in depth and geometry surface have been considered and the simulation has not taken into account the HfO₂-SiO₂ and SiO₂-substrate roughnesses. Other effects, such as the presence of traps in the high-k dielectric (not included yet in the simulator) that could favor Trap Assisted Tunneling through GBs, or different electrical properties between grain and GBs,¹⁷ also could explain the observed differences between the experimental data and the simulations. In fact, in one study, CAFM experimental data and a simulation model that considered different dielectric constants for grains and GBs were used to demonstrate that the faster degradation observed at GBs in HfO₂/SiO_x stacks could be attributed to an enhanced electric field across the SiO_x layer beneath the thinner HfO₂ film at these sites.¹⁷

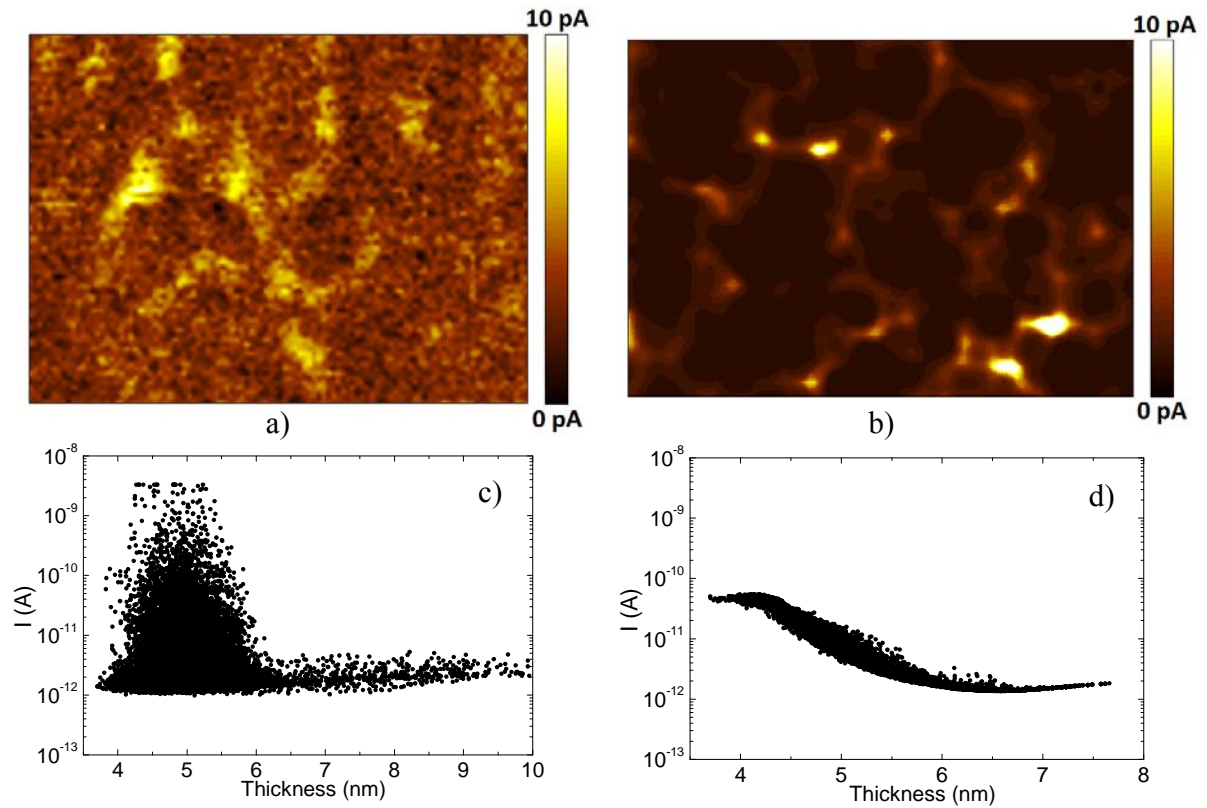


Figure 6. a) Experimental current image corresponding to the topography map in Fig. 3a (area of $300 \times 400 \text{ nm}^2$). The applied bias was 6 V. b) Simulated current image corresponding to the topography map in Fig. 3b (area of $300 \times 400 \text{ nm}^2$). The applied bias was 2 V. c) Experimental current as a function of thickness and d) simulated current as a function of thickness.

IV. SUMMARY AND CONCLUSIONS

In this work, we presented a simulation methodology that allows reproduction of topography AFM images based on several experimental aspects, such as tip radius or tip material. Good agreement was found between the simulations and experimental results. In addition, current through the dielectric stack was calculated from the band diagram at each point on the surface. The current calculation took the morphology and electrical properties of the high-k material and C-AFM tip into consideration. This simulation

method can be very useful for evaluating the unavoidable experimental effects intrinsic to the C-AFM technique.

ACKNOWLEDGMENTS

This work has been partially supported by the Spanish MINECO and ERDF (TEC2013-45638-C3-1-R), and the Generalitat de Catalunya (2014SGR-384).

¹J. Robertson, Rep. Prog. Phys. **69**, 327 (2006).

²A. Asenov, S. Roy, R. A. Brown, G. Roy, C. Alexander, C. Riddet, C. Millar, B. Cheng, A. Martinez, N. Seoane, D. Reid, M. F. Bukhori, X. Wang and U. Kovac, Int. El. Devices Meet 421, (2008).

³A. Bayerl, M. Lanza, M. Porti and M. Nafria, IEEE T. Electron Dev, **11**(3), 495 (2011).

⁴M. Nafria, R. Rodriguez, M. Porti, J. Martin, M. Lanza and X. Aymerich, Int. El. Devices Meet pp 6.3.1 - 6.3.4, (2011).

⁵V. Iglesias, M. Porti, M. Nafria, X. Aymerich, P. Dudek, T. Schroeder and G. Bersuker, Appl. Phys. Lett. **97**, 262906 (2010).

⁶M. Lanza, V. Iglesias, M. Porti, M. Nafria and X Aymerich, Nanoscale Res. Lett. **6**(1), 108 (2011).

⁷V. Yanev, M. Rommel, M. Lemberger, S. Petersen, B. Amon, T. Erlbacher, A. J. Bauer, H. Ryssel, A. Paskaleva, W. Weinreich, C. Fachmann, J. Heitmann and U. Schroeder, Appl. Phys. Lett. **92**, 252910 (2008).

⁸<http://gwyddion.net>

⁹R. Y. Rubinstein and D. P. Kroese, *Simulation and the Monte Carlo Method*, (Wiley, USA, 2008).

¹⁰P. Markiewicz and M. C. Goh, J. Vac. Sci. Technol. B **13**, 1115 (1995).

- ¹¹R. G. Southwick III and W. B. Knowlton, IEEE T. Device Mat. Re. **6**, 2,136, (2006).
- ¹²R. G. Southwick III, A. Sup, A. Jain and W. B. Knowlton, IEEE T. Device Mat. Re. **11**, 2,236, (2011).
- ¹³K. F. Brennan and C. J. Summers, J. Appl. Phys. **61**, 614 (1987).
- ¹⁴B. Jonsson and S. T. Eng, IEEE J. Quantum Elect. Vol. 26, No. 11, (1990).
- ¹⁵W. W. Liu and M. Fukuma, J. Appl. Phys. **60**, 1555 (1986).
- ¹⁶F. A. Noor, M. Abdullah, Sukirno, Khairurrijal, A. Ohta and S. Miyazaki, J. Appl. Phys. **108**, 093711 (2010).
- ¹⁷K. Shubhakar, N. Raghavan, S.S. Kushvaha, M. Bosman, Z. R. Wang, S. J. O'Shea and K.L. Pey, Microelectron Reliab, **54**, 1712, (2014).